Electronic Supplementary Information

Experimental details

Materials characterization. Powder X-ray diffraction (XRD) tests were carried out on a Rigaku Minflex 600 Advance X-ray instrument (Cu Kα radiation, λ = 1.5406 Å) at a voltage of 40 kV and a current of 40 mA. A Nicolet IS50 FTIR spectrometer (Thermo Scientific) was employed to collect the Fourier transform infrared (FTIR) spectra. Field-emission scanning electron microscope (FESEM; Hitachi SU 8010) and transmission electron microscope (TEM; Philips, Tecnai 20 FEI) were used to examine the morphology and structure of the samples. The compositions of the samples were determined by energy-dispersive X-ray spectroscopy (EDS) attached to transmission electron microscope (TEM; Philips, Tecnai 20 FEI) and inductively coupled plasma emission spectrometer (iCAP7400). AC-STEM (aberration-corrected scanning transmission electron microscopy) coupled with four energy dispersive X-ray spectroscopy detectors, were used to examine the morphology and structure of the samples on a ThermoFisher Scientific TEM (Themis Z) working at 300 kV. The HAADF collection angle of imaging was 61 to 200 mrads. X-ray photoelectron spectroscopy (XPS) analysis and Ultraviolet photoelectron spectra were carried out on a PHI Quantum 2000 XPS system with C 1s binding energy (284.6 eV) as the reference and He I excitation (21.22 eV) as the monochromatic light source. N_2 and CO_2 adsorption-desorption isotherms characterizations were conducted on a Micromeritics ASAP2020 under liquid nitrogen (77K) temperature and ice/water mixture temperature (273K), respectively.

The temperature-programmed desorption of H_2 (H_2-TPD) and CO_2 (CO_2-TPD) were performed using a xq-instrument TP-5080 chemisorption analyzer equipped with a TCD detector. For H_2-TPD, the sample was heated from room temperature to 300 °C at a ramping rate of 10 °C min^{-1} and held at 300 °C for 1 h, followed by cooling to 50 °C in a 10% H_2/Ar mixture. After that, the carrier gas was

switched to Ar to remove the weakly adsorbed H_2. Then the temperature was ramping at 10 °C min^{-1} for H_2 desorption. For CO_2-TPD, the sample was heated from room temperature to 300 °C at a ramping rate of 10 °C min^{-1} and held at 300 °C for 1 h, followed by cooling to 50 °C in a 10% H_2/Ar mixture. After that, the carrier gas was switched to Ar to remove the weakly adsorbed H_2. Then the temperature was ramping at 10 °C min^{-1} for CO_2 desorption.

In-situ DRIFT spectra were carried out using a Nicolet iS50FTIR spectrometer (Thermo, U.S.A.) with a liquid-nitrogen-cooled MCT-A detector. Put about 100 mg of the sample (A mixture of 10 mg catalyst and 90 mg KBr) into the sample tank of the stainless-steel vacuum chamber with two pieces of copper mesh at the bottom and compact it. Set up the device according to the setup in the picture above, turn on the condensate water, and add liquid nitrogen toward the liquid N_2 added inlet. Before the experiment, the DRIFTS accessory optics were aligned and optimized. Data collection consisted of 32 scans per spectrum with a resolution of 4 cm^{-1}. Prior to the adsorption measurement of a mixture of CO_2 and H_2 ($V_{H_2}/V_{CO_2}/V_{He}$ = 72: 24: 4), the samples in the in-situ reaction cell were purged with Ar gas for 1 h to remove the water and gas impurities physically adsorbed on the catalyst surface. Subsequently, the reactant gas (2 mL min^{-1} of CO_2 and H_2, 18 mL min^{-1} of Ar) was then introduced into the reaction chamber. The adsorption curves of CO_2 at room temperature were recorded at regular intervals. After that, the background of CO_2 adsorption curve was deducted. Turn on the heater at a rate of 5 °C min^{-1} to 260 °C, then deduct the background, and the changes of intermediates on the catalyst surface were recorded at regular intervals.

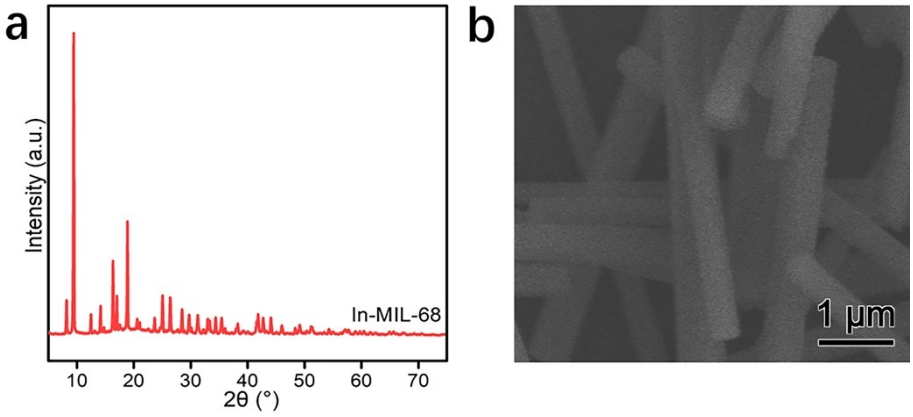

Fig. S1 (a) XRD pattern and (b) FESEM image of In-MIL-68 prisms.

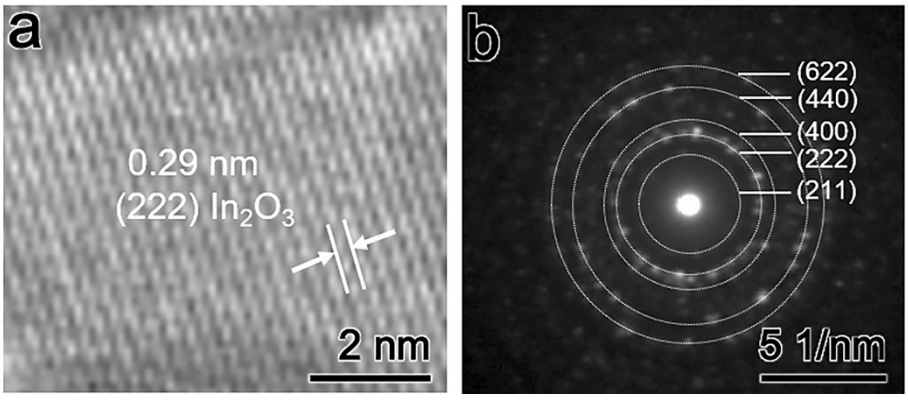

Fig. S2 (a) HRTEM image and (b) SAED pattern of In_2O_3.

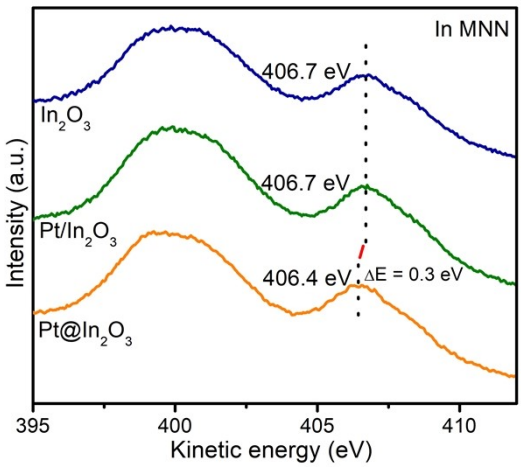

Fig. S3 In MNN Auger spectra of In_2O_3, Pt/In_2O_3 and $Pt@In_2O_3$.

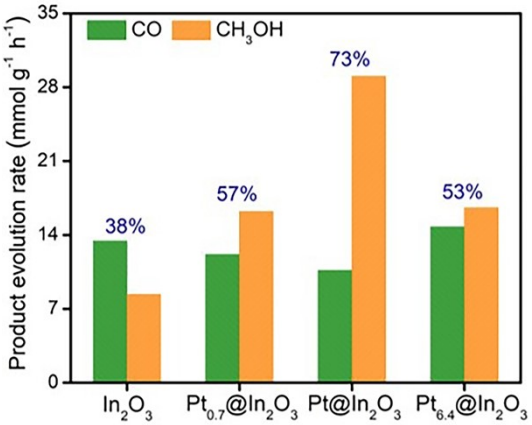

Fig. S4 CO_2 hydrogenation performance of In_2O_3, $Pt_{0.7}@In_2O_3$, $Pt_{6.4}@In_2O_3$ and $Pt@In_2O_3$.

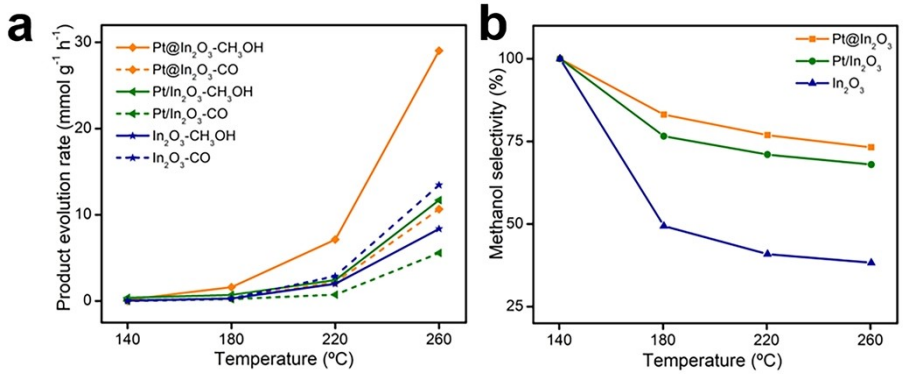

Fig. S5 (a) Product evolution rates and (b) methanol selectivity of In_2O_3, Pt/In_2O_3 and $Pt@In_2O_3$ at different reaction temperatures.

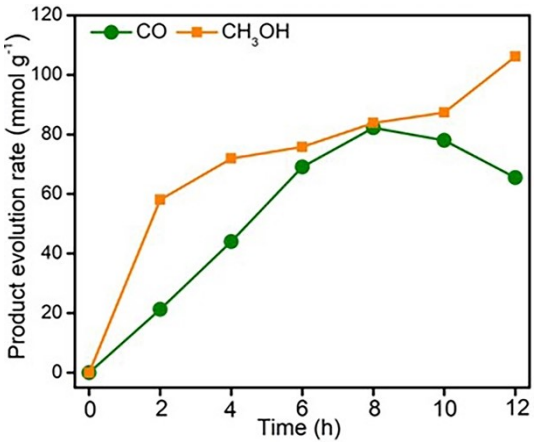

Fig. S6 Long-time catalytic activity of $Pt@In_2O_3$.

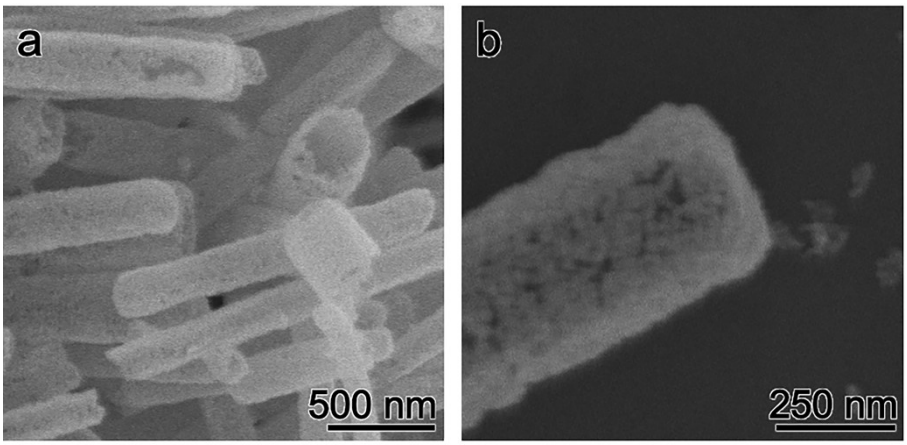

Fig. S7 SEM images of $Pt@In_2O_3$ after reaction.

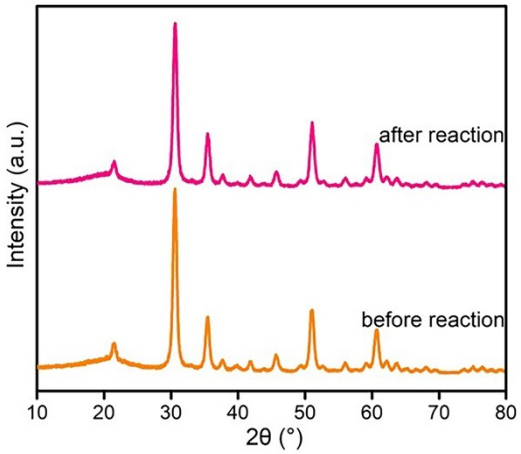

Fig. S8 XRD patterns of $Pt@In_2O_3$ before and after reaction.

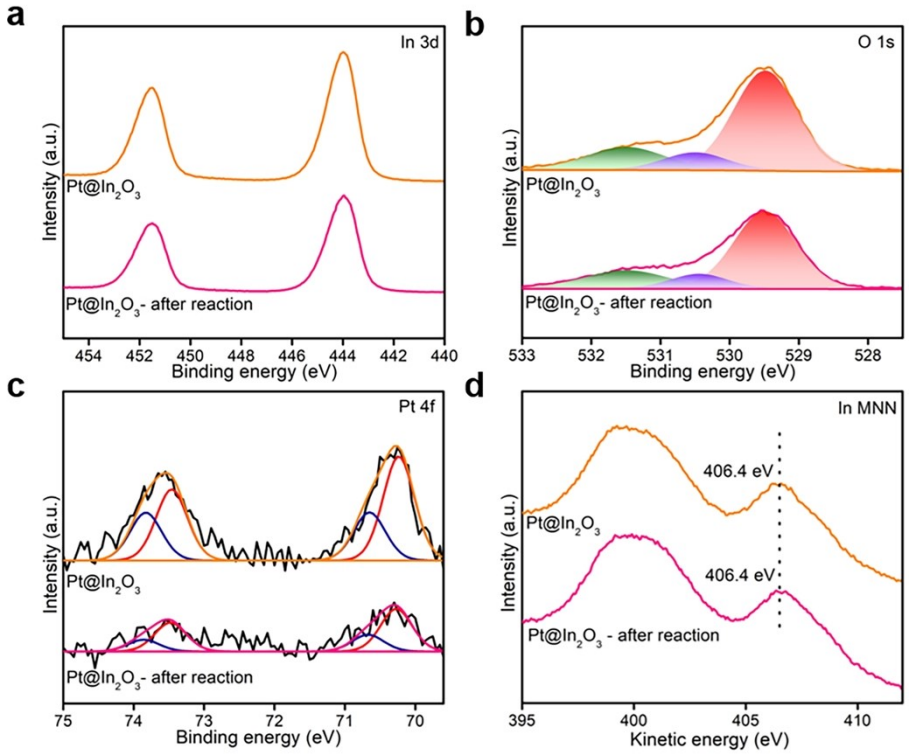

Fig. S9 (a) In 3d, (b) O 1s, (c) Pt 4f XPS spectra and (d) In MNN Auger spectra of $Pt@In_2O_3$ before and after the CO_2 hydrogenation reaction.

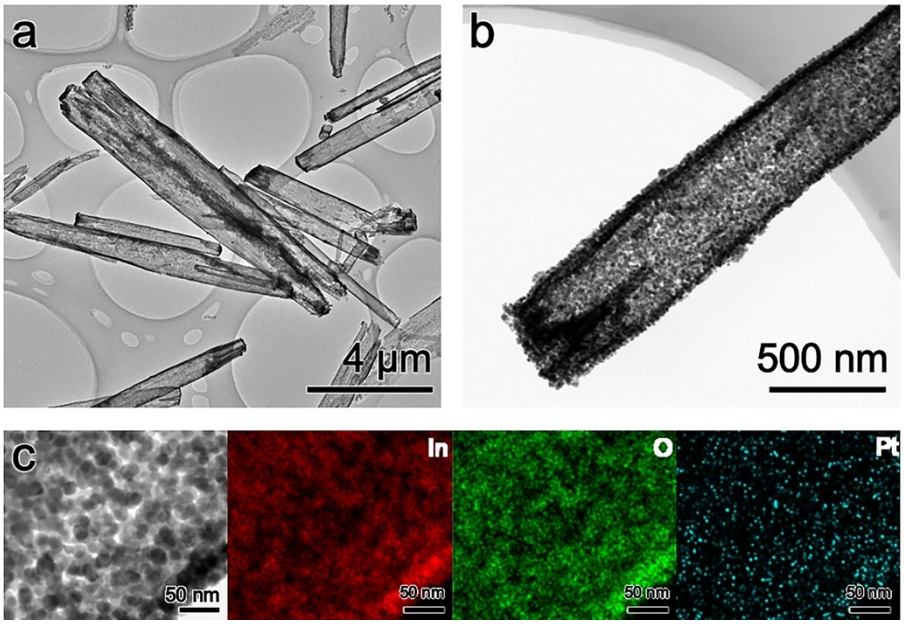

Fig. S10 (a,b) TEM images and (c) EDX maps of $Pt@In_2O_3$ after reaction.

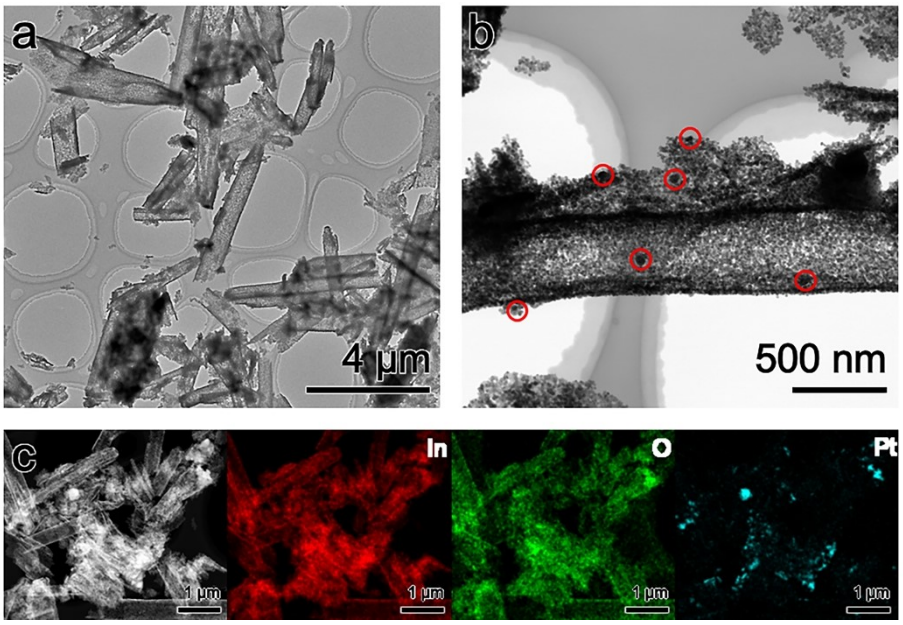

Fig. S11 (a,b) TEM images and (c) EDX maps of Pt/In_2O_3 after reaction.

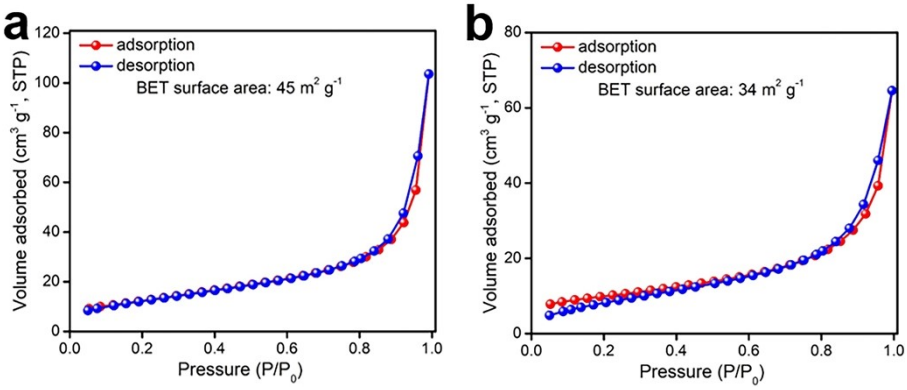

Fig. S12 N_2 sorption isotherms and BET surface area of Pt/In_2O_3 (a) before and (b) after reaction.

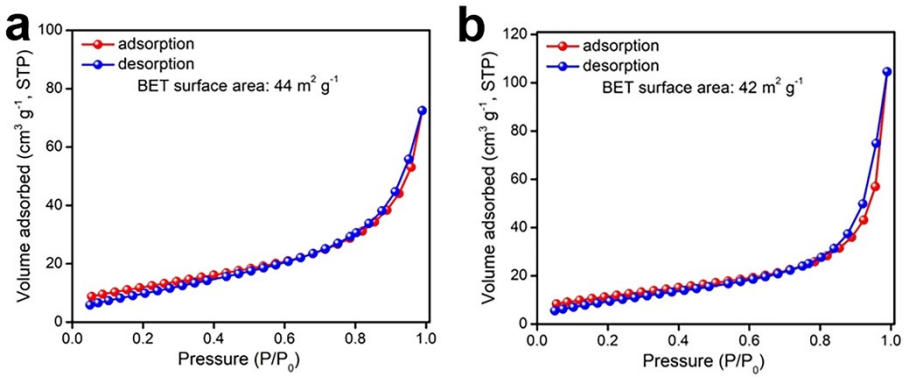

Fig. S13 N_2 sorption isotherms and BET surface area of Pt@In_2O_3 (a) before and (b) after reaction.

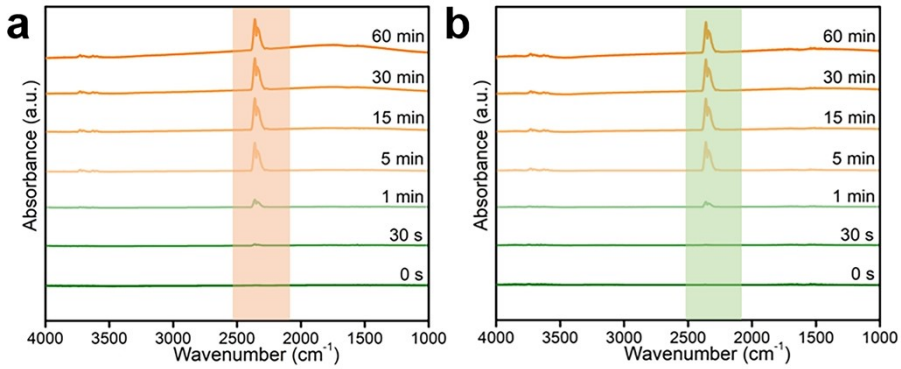

Fig. S14 *In-situ* DRIFT spectra of (a) Pt@In_2O_3 and (b) Pt/In_2O_3 under different CO_2 adsorption times at 25 °C.

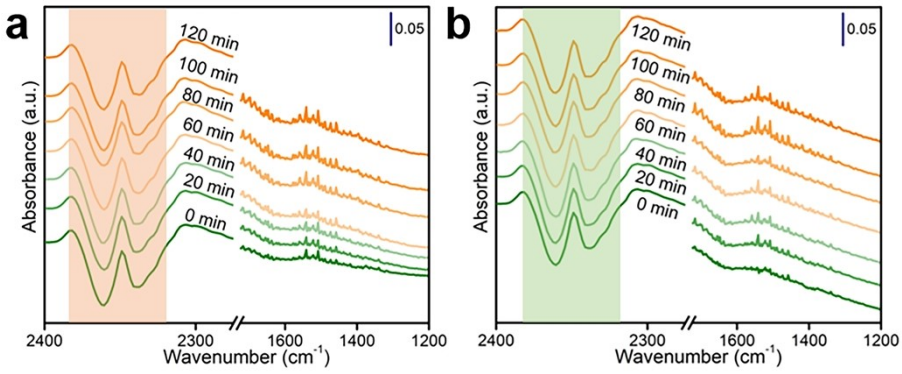

Fig. S15 *In-situ* DRIFT spectra of (a) Pt@In_2O_3 and (b) Pt/In_2O_3 collected at 260 °C for different reaction times in CO_2-saturated atmosphere.

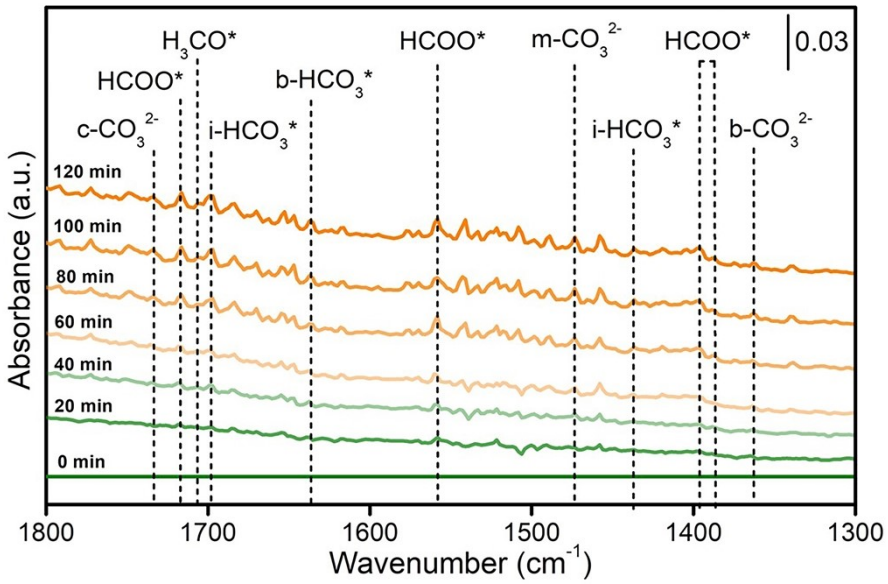

Fig. S16 *In-situ* DRIFT spectra of Pt/In_2O_3 collected at 260 °C for different reaction times in CO_2-saturated atmosphere.

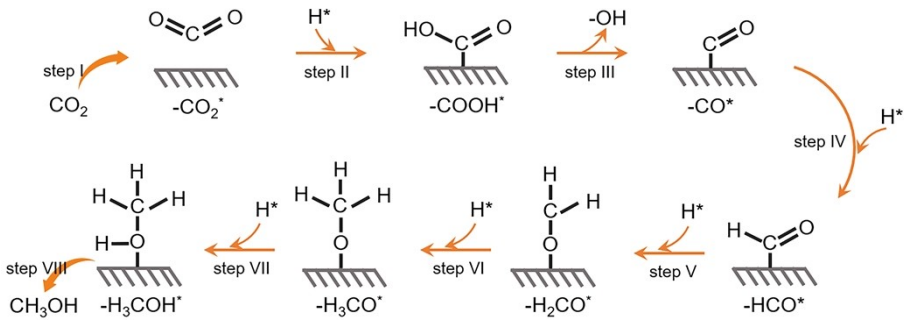

Fig. S17 Schematic illustration of methanol production from CO_2 hydrogenation involving CO as the intermediate over the Pt@In_2O_3 catalyst

Table S1. The CH_3OH generation rate of $Pt@In_2O_3$ in comparative with those of other catalysts in similar In_2O_3-based catalysts.

Catalysts	Pressure (MPa)	Temperature (°C)	Selectivity (%)	Yiled rate (mmol $g_{cat}^{-1} \cdot h^{-1}$)	Ref.
$Pt@In_2O_3$	3	260	73	29.0	This work
Pt/In_2O_3	2	300	56	15.1	1
Pt/In_2O_3	5	300	53	16.9	2
Rh/In_2O_3	5	300	56	17.0	3
Au/In_2O_3	5	300	68	14.7	4
Ni/In_2O_3	5	300	54	17.2	5
$Pd\text{-}P/In_2O_3$	5	300	72	27.6	6
Pd/In_2O_3-CP	5	280	75	19.1	7
$h\text{-}In_2O_3/Pd$	3	295	72.4	16.6	8
$Pd@In_2O_3$	3	295	81.1	13.4	9
Pd/In_2O_3/SBA-15	5	260	84	11.0	10
$h\text{-}In_2O_3$	5	340	78	9.5	11
In_2O_3/ZrO_2	5	300	99.5	9.2	12

Table S2. The content of Pt in each sample determined by ICP-OES.

Sample	Pt content (wt.%)
$Pt_{0.7}@In_2O_3$	0.7
$Pt@In_2O_3$	1.6
$Pt_{6.4}@In_2O_3$	6.4
Pt/In_2O_3	1.6

Supplementary References

1. Z. Han, C. Tang, J. Wang, L. Li and C. Li, *J. Catal.*, 2021, **394**, 236-244.

2. K. Sun, N. Rui, Z. Zhang, Z. Sun, Q. Ge and C.-J. Liu, *Green Chem.*, 2020, **22**, 5059-5066.

3. J. Wang, K. Sun, X. Jia and C.-j. Liu, *Catal. Today*, 2021, **365**, 341-347.

4. N. Rui, F. Zhang, K. Sun, Z. Liu, W. Xu, E. Stavitski, S. D. Senanayake, J. A. Rodriguez and C.-J. Liu, *ACS Catal.*, 2020, **10**, 11307-11317.

5. X. Jia, K. Sun, J. Wang, C. Shen and C.-j. Liu, *J. Energy Chem.*, 2020, **50**, 409-415

6. N. Rui, Z. Wang, K. Sun, J. Ye, Q. Ge and C.-j. Liu, *Appl. Catal., B*, 2017, **218**, 488-497

7. M. S. Frei, C. Mondelli, R. García-Muelas, K. S. Kley, B. Puértolas, N. López, O. V. Safonova, J. A. Stewart, D. Curulla Ferré and J. Pérez-Ramírez, *Nat. Commun.*, 2019, **10**, 3377.

8. Z. Cai, J. Dai, W. Li, K. B. Tan, Z. Huang, G. Zhan, J. Huang and Q. Li, *ACS Catal.*, 2020, **10**, 13275-13289.

9. Z. Cai, M. Huang, J. Dai, G. Zhan, F.-l. Sun, G.-L. Zhuang, Y. Wang, P. Tian, B. Chen, S. Ullah, J. Huang and Q. Li, *ACS Catal.*, 2022, **12**, 709-723.

10. H. Jiang, J. Lin, X. Wu, W. Wang, Y. Chen and M. Zhang, *J. CO_2 Util.*, 2020, **36**, 33-39.

11. S. Dang, B. Qin, Y. Yang, H. Wang, J. Cai, Y. Han, S. Li, P. Gao and Y. Sun, *Sci. Adv.*, 2020, **6**, eaaz2060.

12. O. Martin, A. J. Martín, C. Mondelli, S. Mitchell, T. F. Segawa, R. Hauert, C. Drouilly, D. Curulla-Ferré and J. Pérez-Ramírez, *Angew. Chem. Int. Ed.*, 2016, **55**, 6261-6265.